Brain, Behavior, & Immunity - Health 9 (2020) 100129

Contents lists available at ScienceDirect

Brain, Behavior, & Immunity - Health

journal homepage: www.editorialmanager.com/bbih/default.aspx

Full Length Article

The SMYD1 and skNAC transcription factors contribute to neurodegenerative diseases

R. Dayne Mayfield [a,b,d], Li Zhu [c,d], Tyler A. Smith [b], Gayatri R. Tiwari [a], Haley O. Tucker [d,*]

[a] Waggoner Center for Alcohol and Addiction Research, The University of Texas at Austin, Austin, TX, 78712, USA
[b] Department of Neuroscience, The University of Texas at Austin, Austin, TX, 78712, USA
[c] Department of Pathology, Lokey Stem Cell Research Building, 265 Campus Drive, Stanford, CA, 94305, USA
[d] Department of Molecular Biosciences, The University of Texas at Austin, 1 University Station A5000, Austin, TX, 78712, USA

ARTICLE INFO

Keywords:
Transcriptional regulation
SMYD1 and skNAC
Neuroinflammatory disease

ABSTRACT

SMYD1 and the skNAC isoform of the NAC transcription factor have both previously been characterized as transcription factors in hematopoiesis and cardiac/skeletal muscle. Here we report that comparative analysis of genes deregulated by SMYD1 or skNAC knockdown in differentiating C2C12 myoblasts identified transcripts characteristic of neurodegenerative diseases, including Alzheimer's, Parkinson's and Huntington's Diseases (AD, PD, and HD). This led us to determine whether SMYD1 and skNAC function together or independently within the brain. Based on meta-analyses and direct experimentation, we observed SMYD1 and skNAC expression within cortical striata of human brains, mouse brains and transgenic mouse models of these diseases. We observed some of these features in mouse myoblasts induced to differentiate into neurons. Finally, several defining features of Alzheimer's pathology, including the brain-specific, axon-enriched microtubule-associated protein, Tau, are deregulated upon SMYD1 loss.

1. Introduction

SET and MYND Domain 1 (SMYD1) is a transcription factor characterized extensively in hematopoietic cells, cardiac/skeletal muscle (where it is essential for embryonic survival) (Yahalom et al., 2018; Tracy et al., 2018; Franklin et al., 2016; Murayama et al., 2015; Rasmussen et al., 2015; Rasmussen and Tucker, 2018; Fujii et al., 2016; Hsia and Zon, 2005; Tan et al., 2006; Jing and Zon, 2011; Paik and Zon, 2010) and in endothelial cells where it acts as a SRF-interacting partner required for angiogenesis (Ye et al., 2016). SMYD1 belongs to a family of three orthologous isoforms, SMYD1A (employed throughout this study and termed SMYD1), SMYD1B, and SMYD1C whose SET domains are split by a MYND protein-interaction domain [reviewed in (Tracy et al., 2018)]. In addition to its role as a TF, SMYD1A and B possess histone methyltransferase activity by catalyzing methylation of histone H3 lysine K4 (H3K4m3), H3K9m1 and potentially other histone methylation marks during cardiac remodeling (Tracy et al., 2018). SMYD1 also monomethylates a single lysine within the hematopoietic stress response factor, Tribbles3/TRB3 (Nie et al., 2017).

SMYD1 interacts with the cardiac/skeletal and hematopoietic-specific TF skNAC, an alternatively spliced isoform of NACA (Yotov and St-Arnaud, 1996), which is required for transactivation of Myoglobin (MB) (Sims et al., 2002). Consistent with their physical interaction, the temporal and spatial expression patterns of skNAC are almost identical to those of SMYD1 (Sims et al., 2002; Raval et al., 2012; Park et al., 2010). *Smyd1* and *Sknac* mutant embryos exhibit similar gene dysregulation (Park et al., 2010).

Here we employed global gene expression and integrated KEGG database pathway analyses (KanehisaSato et al., 2016) to determine what targets are deregulated by SMYD1, skNAC or both in C2C12 myocytes following three days of differentiation to myoblasts. As anticipated, we observed numerous hematopoietic and cardiac/skeletal muscle targets, including MB. However, we observed numerous others that showed no obvious hematopoietic or cardioskeletal phenotypes. Unexpectedly, these included a number of highly deregulated transcripts characteristic of neurodegenerative diseases, including Alzheimer's (AD), Parkinson's (PD) and Huntington's (HD) Diseases (readdressed in Results and Discussion). The cause of each of these diseases is death of neurons and other

* Corresponding author. Molecular Biosciences, Institute for Cellular and Molecular Biology, University of Texas at Austin, 1 University Station A5000, Austin, TX, 78712, USA.
E-mail address: haleytucker@austin.utexas.edu (H.O. Tucker).

https://doi.org/10.1016/j.bbih.2020.100129
Received 3 August 2020; Received in revised form 10 August 2020; Accepted 12 August 2020
Available online 1 September 2020

cells within the brain, and each can affect different regions of the brain (Smyth, Grosser et al., 2820; Lezi and Swerdlow, 2012; CanuSarasso et al., 2018; O'Brien et al., 2017; Bray, 2020; Elkouzi, Vedam-Mai et al., 2019). In essence, Alzheimer's destroys memory, while Parkinson's and Huntington's affect movement. Each of these diseases is progressive, debilitating and incurable (Smyth, Grosser et al., 2820; Lezi and Swerdlow, 2012; CanuSarasso et al., 2018; JT O'Brien et al., 2017; Bray, 2020; Elkouzi, Vedam-Mai et al., 2019).

The above observations, coupled with the finding that mouse knockouts of SMYD1 paralogues SMYD4 and SMYD5 each resulted in significant behavioral phenotypes (GiauSenanarong et al., 2019), led us to hypothesize that SMYD1 and skNAC function together, not only in hematopoietic and cardiovascular/skeletal tissues, but in neuronal cells as regulators of genes disrupted in AD, PD and HD. This hypothesis was strengthened by our observation that SMYD1 and skNAC are expressed strongly within the cortical striata of human brains, weakly in the cortical striata of mouse brains and within the cortical striata of transgenic models of each of the inflammatory diseases noted above. We show that both SMYD1 and skNAC are expressed in C2C12 myocytes induced to differentiate to neurons, but only SMYD1 is essential for this process. Finally, ether together or individually, SMYD1 and skNAC regulate several defining components of neurodegeneration, and particularly Alzheimer's pathology, including the brain-specific, axon-enriched microtubule-associated protein, Tau.

These findings open heretofore unanticipated potential for SMYD1 and skNAC function in neurodegenerative disorders that in 2019 exceeded $290 billion in treatment and hospitalization (Alzheimer's Association Report, 2019).

2. Materials and methods

2.1. Mice and animal husbandry

Mice were bred and housed in the pathogen-free animal facility of the University of Texas. All experiments received approval from the Institutional Animal Care and Use Committees (Protocol ID AUP-2012-00169). Approximately 3 week old transgenic (TG) mouse models were purchased from the Jackson Laboratory. Further details are provided in S-Methods.

2.2. Cell culture and production of stable cell lines

We employed C2C12 (purchased from ATCC). Phoenix A cells were the kind gift of Dr. Gary Nolan. Production of recombinant retroviral constructs and infection of cell lines was performed as detailed in S-Methods and as described at http://www.stanford.edu/group/nolan/protocols/pro_helper_dep.html. Briefly, Phoenix A cells were plated and then transfected with retroviral construct DNA using Fugene 6 reagent (Roche). Approximately 48 h post-transfection, supernatants were selected with 3 μg/ml puromycin and split at 80% confluency.

2.3. Mammalian expression

Vectors pBK-CMV-SMYD1A, pBK-CMV-SMYD1B, pBKCMV-SMYD1c and pBK-CMV-SMYD1B-YND-mutant were described previously (Rasmussen et al., 2015; Rasmussen and Tucker, 2018). pSilencer5.1-U6-SMYD1-(sh-RNA), pSilencer5.1-U6-skNAC-(sh-RNA) and pSilencer5.1-U6-Scramble (sh-RNA) were generated with software (shRNA selector) available at http://hydra1.wistar (Upenn. edu/Projects/shRNA/shRNAindex.htm). Transient transfections were performed with FuGENE 6 reagent according to the manufacturer's instructions.

2.4. Antibodies, western blotting and immunohistochemistry (IHC)

Anti-SMYD1 3b2a monoclonal antibody (mAb) was described previously (Sims et al., 2002). Rabbit anti-skNAC polyclonal antibody (UT143) was generated as detailed in S-Methods by Cocalico Biologicals. Anti-FLAG M2 mAb is from Sigma (cat #F3165); anti-Acetylcholinesterase (CAT) biotinylated monoclonal (HR2) and anti-Neuron-Specific beta-III Tubulin (NST) biotinylated monoclonal Ab (Catalog # BAM1195) were each purchased from Invitrogen (Catalog # MA3-042) Filamentous actin (F-actin) was stained with FITC-conjugated phalloidin (Sigma-Aldrich; St. Louis, MO). Nuclei were labeled with 4′-6-diamidino-2-phenylindol (DAPI). For immunoprecipitation, we employed protein-A immobilized on Sepharose CL-4B (cat #P3391) as detailed in S-Methods.

Our Western blotting procedure, described previously (Rasmussen et al., 2015; Rasmussen and Tucker, 2018), was performed on 12.5% SDS-PAGE with the above mentioned commercial and home-generated Abs as detailed in S-Methods. For IHC, mice were anesthetized, perfused intracardially with ice cold HBSS and drop fixed overnight in 4% paraformaldehyde (PFA). Brain sections (25μm) were collected by cryostat, mounted and developed with antibodies noted above as detailed in S-Methods.

2.5. Retroviral shRNA silencing

PSilencer5.1-U6-SMYD1 (shRNA), pSilencer5.1-U6-skNAC(shRNA) and pSilencer5.1-U6-Scramble (shRNA) were generated as follows: The shRNA target sequences were selected by employing siRNA selector (http://hydra1.wistar.upenn.edu/Projects/siRNA/siRNAindex.htm). Design Tool (Ambion) was used to convert the target sequences into hairpin shRNA-encoding DNA oligonucleotide sequences. These oligonucleotide sequences were annealed and ligated into pSilencer 5.1 Retro vector (Ambion).

2.6. Microarray analysis

C2C12 myoblasts or skNAC-shRNA KD-transduced C2C12 myoblasts were induced for 3 days in culture via serum withdrawal to myoblasts as described previously (Sims et al., 2002). Total RNA was purified with TRIzol reagent (Life Technologies, Inc. Rockville, MD) and hybridized to DNA-spotted arrays (printed in house as described in: Jing and Zon, 2011; Paik and Zon, 2010). Details of microarray, hybridization, scanning, creation of image files and analyses are provided in S-Methods. Differentially expressed genes (nominal $p < 0.05$) of SMYD1 or skNAC vs. their respective WTs were determined and their datasets were analyzed using the Ingenuity Pathway Analysis (IPA) 'Core Analysis' utility (Chen et al., 2013; Kuleshov et al., 2016; Meeson et al., 2001) and displayed as volcano plots as detailed in S-Methods.

2.7. Conversion of myoblasts to neurons

C2C12 cells were converted to neurons via a method described in detail in S-Methods. Briefly C2C12 myocytes were converted to myoblasts as previously described (Yotov and St-Arnaud, 1996), incubated for 3 days in a media containing 3 mm Neuodazine (Nz; LGC Standards, ICRS0247). The media was replaced every 2 days with 4 mm Nz prior to their harvest and analysis at day 6.

2.8. Purification of mouse subcortical regions

Mice were anesthetized, perfused intracardially with HBSS and drop-fixed overnight in 4% paraformaldehyde (PFA). Brain sections (25μm) were collected using a cryostat, mounted onto charged slides and then stored at −80 °C until use. Brain sections were rehydrated in PBS, blocked for 1 h at RT in 10% calf serum, 0.2% Triton X-100, in 1× PBS prior to further analyses.

2.9. Dendritic tree reconstruction

Briefly, C2C12 neurons were sliced into 10 mm thick blocks and stained with a FD Rapid GolgiStain™ kit (FD NeuroTechnologies, Ellicott City, MD, USA). The blocks were sectioned using a cryomicrotome

(Microm Thermo Scientific, Walldorf, Germany) to ~200 μm and then were mounted on gelatin-coated microscope slides. Approximately 100 medium spiny neurons for each genotype were three-dimensionally reconstructed using Neurolucida software version 10 (MBF–Bioscience, Williston, ND, USA) with a system composed of a z-axis motorized Olympus BX61 microscope equipped with x-y motorized stage guided by a MAC5000 stage controller (Ludl Electronic Products Ltd, Hawthorne, NY, USA). Projections were calculated using Neurolucida software version 10. Levels along the rostro-caudal striatal axis where measured, and reconstructions were performed with maximum density of dendritic spines (lacking incomplete impregnation) reconstructed.

2.10. RT-qPCR and endpoint PCR

RT-qPCR was conducted as previously described (Hsia and Zon, 2005) and detailed in S-Methods. Briefly, total cellular RNA was isolated using an RNeasy Mini Kit (QIAGEN, Santa Clara, CA), cDNA synthesized with qScript cDNA supermix (Quanta), and RT-qPCRs were performed using PerfeCTa SYBR Green FastMix (Quanta) with 1 μL of 20X-diluted cDNA generated from 500 ng of total RNA. RT-qPCR primers, designed to amplify the junction between two exons, are listed in S-Fig. 2. CT values were normalized against *Gapdh*. The normalized level of mRNA was determined as 2^{-Ct} (GOI)/2^{-Ct} (CTL), where Ct is the threshold cycle, GOI is the transcript of interest, and CTL is the housekeeping control (assuming that Ct is inversely proportional to the initial concentration of mRNA and that the amount of product doubles with every cycle). PCR products were analyzed via electrophoresis over agarose or SDS-PAGE. Primers designed using Primer 3 software for SMYD1: 5′-GTGAAGAACGCAAGAGGCAGCT-3'; 5′-CTCCTTCACCACTTCCTGAGAG-3′ and for skNAC: 5′- ATTCCACC-CAGGCAACCACACA-3'; 5′-TGTAACCTGCCGAAGACCCAGT.

3. Results

3.1. Determination of SMYD1 and skNAC transcriptional targets in myoblasts

We employed global gene expression analyses to determine SMYD1 and skNAC transcriptional targets in C2C12 myocytes following their differentiation to myoblasts. We employed shRNA-mediated knockdown (KD) of SMYD1 or skNAC. Their KD efficiencies, as shown in S-Fig. 1, were robust. Differential expression (DE) analysis performed in two independent replicates yielded 1672 significantly (nominal $p < 0.05$) altered transcripts for SMYD1 loss and 1209 significantly (nominal $p < 0.05$) altered transcripts for skNAC KD with respect to wildtype (WT) controls (summary statistics and transcripts listed in S-Tables 1 and 2). DE genes were submitted to Ingenuity Pathway Analysis (IPA) (Chen et al., 2013) to identify molecular pathways. To identify networks, we overlaid and merged SMYD1 and skNAC KDs via the "fold-change" (FC) algorithm as logFC expression values (Chen et al., 2013; Kuleshov et al., 2016).

Using the Ingenuity Knowledge Base algorithm (Chen et al., 2013), association between SMYD1 and skNAC networks were identified with the IPA "Grow" tool (Chen et al., 2013), in which a maximum of 20 target molecules for each factor were connected to targets within their respective networks. We employed default settings (Chenet al., 2013; Kuleshov et al., 2016) for all IPA pathway functions. We then performed KEGG pathway analyses (KanehisaSato et al., 2016) employing *Enrichr*^{TM} (Kuleshov et al., 2016)—a comprehensive resource for curated gene sets and a search engine that accumulates biological knowledge for further discovery.

3.2. SMYD1 and skNAC loss deregulates factors involved in heart and skeletal muscle development, cardiac muscle contraction, inflammatory responses and TCA cycle

We first analyzed differential gene expression and as represented in Volcano plots (Fig. 1). Genes deregulated by SMYD1 KD (left panel) are shown with nominal p values < 0.004 (blue dots) and log2-fold changes >1.3 (green dots). Genes deregulated by skNAC KD (right panel) are shown with nominal p values < 0.003 (blue dots) and log2-fold changes >1.4 (green dots). Genes that pass both the cutoff for log2FC and p value are shown as red dots, whereas genes that did not reach these criteria are indicated in gray. S-Fig. 2B, displays the IPA network association between SMYD1, MB, and skNAC (in blue). The input data included nominally significant genes ($p < 0.05$) for SMYD1 or skNAC KD vs. C2C12 myoblast WT.

3.3. SMYD1 and skNAC regulate neurogenic factors implicated in neurodegerative diseases

We observed numerous KEGG pathways significantly deregulated, including heart/skeletal muscle development and cardiac muscle contraction (Table 1, S-Fig. 2 and data not shown). This was not unexpected, given that SMYD1 regulates skNAC, which, in turn, regulates MB (C. Li et al., manuscript under submission); MB, in turn, supplies ferrous iron (haem) to numerous pathways within cardiac and skeletal muscles of all vertebrates (Meeson et al., 2001).

However, totally unexpected was our finding that loss of SMYD and skNAC led to significant deregulation of genes typically associated with neurodegenerative diseases. Foremost of the SMYD1 GO pathways was Alzheimer's Disease (AD), the most common cause of dementia ($p \leq$ 1.48E-11, Table 1) (Smyth, Grosser et al., 2820; Elkouzi, Vedam-Mai et al., 2019). Loss of SMYD1 also significantly deregulated a number of genes typically expressed in Parkinson's ($p \leq 1.37E-9$) and in Huntington's ($p \leq 1.41E-7$) Diseases. Loss of skNAC also deregulated each of these pathways, but to a more modest extent than SMYD1: Alzheimer's ($p \leq 2.93E-6$), Huntington's ($p \leq 3.29–4$) and Parkinson's ($p \leq 1.37E-3$) (Table 1).

As shown in Table 1 and the Volcano plot of Fig. 2, transcripts common to each of the neurodegenerative diseases included Cyclooxygenase (COX) isoforms, involved in the conversion of arachidonic acid to the prostaglandin precursor of prostaglandins (Smyth, Grosser et al., 2820); NDUFA isoforms, which function in a complex within the mitochondrial electron transport chain downstream of COX, which is deregulated in AD, PD, and HD (Lezi and Swerdlow, 2012); and ATPase isoforms which drive the electron transport chain and have been associated with Aβ plaque burden in Alzheimer's (Holper et al., 2019).

These and other deregulated neurodegenerative transcripts are readdressed in detail below.

3.4. SMYD1 and skNAC accumulate in human brains within a region implicated in neurodegenerative diseases

The above results were unsuspected since all previous publications had detected SMYD1 and skNAC exclusively in developing or mature cardiomyocytes, endothelial cells, skeletal muscle myoblasts and myocytes (Yahalom et al., 2018; Tracy et al., 2018; Franklin et al., 2016; Murayama et al., 2015; Rasmussen et al., 2015; Rasmussen and Tucker, 2018; Fujii et al., 2016; Hsia and Zon, 2005; Tan et al., 2006; Jing and Zon, 2011; Paik and Zon, 2010; Ye et al., 2016), or in the case of SMYD1C, CD8 T cells (Nie et al., 2017).

We searched the literature, and while we found no evidence for SMYD1 and/or skNAC in the mouse brain, we did find evidence for both in the human brain (Holper et al., 2019; Lein et al., 2007; Oh et al., 2014; Miller et al., 2017; Hawrylycz et al., 2012). Fig. 2A and B displays our meta-analyses of samples of four normal human brains in which both SMYD1 and skNAC were identified by *in situ* RNA hybridization (in red) within the cerebral cortex. SkNAC is expressed more diffusely, particularly within the telencephalon (S-Fig. 2) (Lein et al., 2007; Oh et al., 2014; Miller et al., 2017; Hawrylycz et al., 2012). But both reside, in a near overlapping fashion, within the subcortex of normal human donors (Fig. 2A and B). The subcortex constitutes a group of diverse neural formations deep within the brain, which include the thalamus, the hypothalamus and the striatum (Uddin and Ghulam, 2018). As shown in

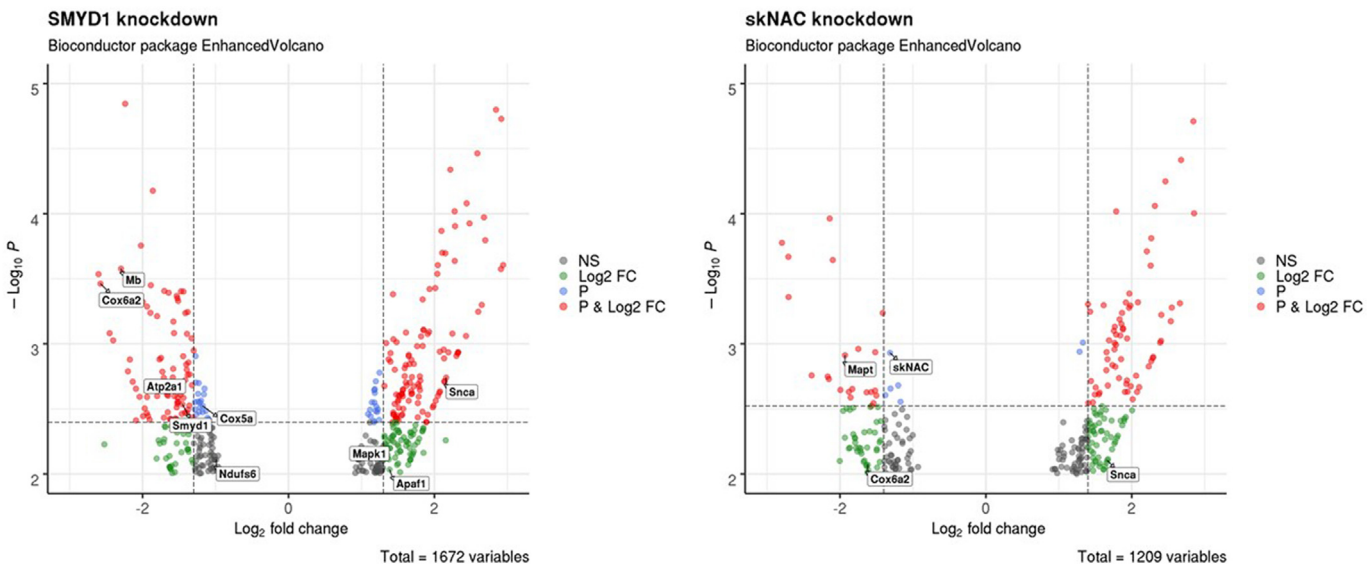

Fig. 1. Neuroinflammatory transcriptional targets of SMYD1 and skNAC in C2C12 myoblasts. Global gene expression analyses were performed following KD of SMYD1 and skNAC in C2C12 myoblasts following 3 days of differentiation. A complete data set comprising non-immunoinflammatory targets is presented as S-Fig. 3. Neuroinflammatory targets constituting the major focus of this report are provided here. Volcano plots shown for differential gene expression of deregulated transcripts resulting from SMYD1 KD (left panel) and skNAC KD (right panel) Genes symbols are shown for PCR-validated genes (see Table 2). Nominal p values < 0.004 and < 0.003 are shown as blue dots for SMYD1 KD and skNAC KD, respectively; and Log2 fold changes >1.3 and > 1.4 are shown as green dots for SMYD1 KD and skNAC KD, respectively. Genes that pass both the cutoff for log2FC and p value are shown as red dots. Gray dots were not significant. **B.** IPA network displaying the association between SMYD1, MB, and skNAC labeled in blue. The input data included nominally significant genes ($p < 0.05$) for SMYD1 vs. WT and skNAC vs. WT. Transcripts highlighted in green are down-regulated and in red are up-regulated based on the overlaid logFC values carrying a negative value or a positive value, respectively. The intensity of green and red molecule colors indicates the magnitude of down- or upregulation. Solid lines indicate direct interaction, whereas dashed lines indicate indirect interactions as supported by information in the Ingenuity knowledge base. **C.** Molecule types/shapes. Lines (dotted and straight) indicate upstream and downstream relationships. (For interpretation of the references to color in this figure legend, the reader is referred to the Web version of this article.)

Fig. 2C, significant levels of SMYD1 (in red) and skNAC (in green) appear to localize closely within the striatum (readdressed below).

In early disease staging, detection of markers of AD extend randomly throughout the brain; ie, degeneration follows a predictable, nonrandom pattern (Hawrylycz et al., 2012; Arendt et al., 2018). The initial sites of degeneration are ill-defined. While controversial (Keller et al., 2018; Arendt et al., 2018), the prevailing concept is that the disease originates within subcortical regions such as locus coeruleus or nucleus basalis of Meynert (reviewed in (Arendt et al., 2018), (GuptaLee et al., 2019)). The hallmark of HD is massive loss/disruption of the medium spiny neurons of the striatum. Early and diffuse cortical and subcortical neurodegeneration underlies the pathology (reviewed in Myers and McGonigle, 2019). PD patients show distributed alteration of temporal variability. However, the variability showing the highest correlation with clinical score is associated with the subcortical network reviewed in Jankowsky et al., 2004.

3.5. Mouse models of neuroinflammatory diseases

The above transcriptional and localization data encouraged us to analyze SMYD1 and skNAC under conditions of ongoing neuroinflammatory disease. As a first step toward this end, we selected the best available transgenic (TG) mouse models for AD, HD and PD.

Several models of AD are available (reviewed in 46). Most incorporate mutations within amyloid precursor protein (APP) and/or presenilin (PSEN). We elected to assess APP/PS1 double Tg mice (Pickrell et al., 2015) (this and other mutant strains detailed in Materials and Methods) which express chimeric mouse/human APP protein (Mo/HuAPP695swe) and a mutant human PSEN (PS1-dE9) (Konnova et al., 2018). Both genes are directed to CNS neurons. Both mutations are associated with early-onset Alzheimer's disease.

There are several categories of TG mice that carry the distinguishing feature of HD—CAG repeats of varying length within the mouse *Huntingtin* (*Htt*) genomic locus (Goldberg et al., 2003). Preferred are Knock-In (KI) models, in which the HD mutation is replicated by directly engineering CAG repeats of varying length. Toward this end, we employed the zQ175 KI allele in which the human *Htt* exon 1 carrying an ~190 amino acid CAG repeat tract replaces the murine *Htt* exon 1 (Brüggemann et al., 2013). Numerous studies of HD disease pathogenesis and assessment of potential therapeutic interventions have employed these KI mice (reviewed in 46).

While an ultimate mouse model that address all Parkinson's-related questions is yet to be developed, a number of existing models are useful in answering specific questions (reviewed in 46). The PARK loci, recently identified by GWAS, are highly favored, and we chose one—the homozygous *Parkin* (Park2tm1Shn) KO (Konnova et al., 2018). Parkin mice harbor mutation of the exon most commonly observed in human autosomal recessive juvenile Parkinsonism patients (Brüggemann et al., 2013) and have been employed broadly in neurobiological research (Maiti et al., 2018).

3.6. The SMYD1-skNAC complex accumulates within the subcortex of normal and neuroinflammatory transgenic mouse models

We obtained, bred and analyzed each of the TG mouse models discussed above. At ~6 weeks of age, we isolated the subcortical layers of TG and WT littermate control brains to determine if, as in the human, SMYD1 and skNAC accumulate. If so, do they form heterodimeric complexes as they do in heart and skeletal muscle (Sims et al., 2002; Raval et al., 2012).

Briefly, mice models of Alzheimer's Disease (TG-AD), Huntington's Disease (TG-HD) and Parkinson's Disease (TG-PD) as well as WT controls were transcardially perfused using ice cold Hank's balanced salt solution (HBSS) and the brains were minced. Subcortical enrichment was achieved using a validated protocol (Kim et al., 2016a) of subsequent enzymatic dissociation, density gradient separation, and magnetic bead sorting as

Table 1

KEGG pathway analyses identification of diseases and molecules deregulated by loss of SMYD1 or skNAC. Gene ontology (GO) analysis were performed with *Enrichr*^{TM} (Kuleshov et al., 2016; Meeson et al., 2001). Pathways significantly deregulated included targets predicted to be deregulated in Alzheimer's, Parkinson's and Huntington's Diseases.

Enrichr pathway analysis: KEGG SMYD1 KD						
Term	Overlap	P-value	Adjusted P-value	Z-score	Combined Score	Genes
Alzheimer disease	38/175	1.48E-11	3.98E-09	−1.16	28.92	COX7B; NDUFA11; COX4I1; NDUFA10; ATP5A1; NDUFB2; ATP2A2; ATP2A1; COX7A2; ATP5G3; ATP5H; PSEN1; COX5B; ATP5O; COX6A2; COX5A; ATP5G1; UQCRH; RTN4; APH1A; ATP5D; MAPK1; NDUFV2; SNCA; APAF1; NDUFA2; SDHA; SDHB; COX7A2 L; NDUFS7; NDUFS6; NDUFAB1; UQCRC1; CYCS; UQCRC2; MAPT; ATF6; CALM2
Thermogenesis	44/231	3.94E-11	5.30E-09	−1.29	30.89	ATF2; COX7B; NDUFA11; COX4I1; NDUFA10; COX17; ATP5A1; NDUFB2; COX7A2; ATP5G3; ATP5H; COX5B; ATP5O; COX6A2; COX5A; ATP5G1; UQCRH; ACTB; RPS6KA3; CPT2; CREB3L2; ATP5D; SLC25A20; NDUFV2; COX10; MAP2K3; ACTL6B; RPS6; NDUFA2; ACSL5; FRS2; ARID1A; SDHA; SDHB; ARID1B; COX7A2 L; RPS6KB1; NDUFS7; NDUFS6; NDUFAB1; GNAS; UQCRC1; GRB2; UQCRC2
Oxidative phosphorylation	30/134	9.34E-10	8.38E-08	−1.23	25.56	ATP6V1 A; COX7B; NDUFA11; COX4I1; NDUFA10; COX17; ATP5A1; NDUFB2; COX7A2; ATP5G3; ATP5H; COX5B; ATP5O; COX6A2; COX5A; ATP5G1; UQCRH; ATP5D; ATP6V1G3; NDUFV2; COX10; NDUFA2; SDHA; SDHB; COX7A2 L; NDUFS7; NDUFS6; NDUFAB1; UQCRC1; UQCRC2
Parkinson disease	31/144	1.37E-09	9.23E-08	−1.32	26.85	COX7B; NDUFA11; COX4I1; NDUFA10; ATP5A1; NDUFB2; COX7A2; ATP5G3; ATP5H; COX5B; UBE2J2; ATP5O; COX6A2; COX5A; ATP5G1; UQCRH; ATP5D; NDUFV2; SNCA; APAF1; NDUFA2; UBE2G2; SDHA; SDHB; COX7A2 L; NDUFS7; NDUFS6; NDUFAB1; UQCRC1; CYCS; UQCRC2
Huntington disease	33/192	1.41E-07	7.57E-06	−1.13	17.83	COX7B; DCTN2; NDUFA11; COX4I1; DCTN4; NDUFA10; CLTC; ATP5A1; NDUFB2; COX7A2; ATP5G3; ATP5H; COX5B; ATP5O; COX6A2; COX5A; ATP5G1; UQCRH; POLR2A; CREB3L2; ATP5D; NDUFV2; APAF1; NDUFA2; SDHA; SDHB; COX7A2 L; NDUFS7; NDUFS6; NDUFAB1; UQCRC1; CYCS; UQCRC2
Cardiac muscle contraction	19/78	2.71E-07	1.22E-05	−2.20	33.22	COX7B; TPM2; COX4I1; TNNC1; TPM1; ATP2A2; COX7A2; ATP1B3; ATP1A1; COX5B; ATP1B1; COX6A2; COX5A; UQCRH; CACNB3; COX7A2 L; SLC9A6; UQCRC1; UQCRC2
Non-alcoholic fatty liver disease (NAFLD)	27/151	8.46E-07	3.25E-05	−1.36	18.96	COX7B; NDUFA11; IRS1; COX4I1; NDUFA10; NDUFB2; COX7A2; COX5B; COX6A2; COX5A; UQCRH; MAPK8; AKT2; RAC1; NDUFV2; NDUFA2; SDHA; SDHB; EIF2S1; ITCH; COX7A2 L; NDUFS7; NDUFS6; NDUFAB1; UQCRC1; CYCS; UQCRC2
Citrate cycle (TCA cycle)	10/32	1.77E-05	5.94E-04	−2.46	26.94	CS; ACLY; SUCLA2; IDH3G; IDH1; OGDH; ACO2; SDHA; SDHB; IDH3A
Adrenergic signaling in cardiomyocytes	20/148	1.06E-03	2.95E-02	−1.44	9.86	CAMK2B; ATF2; TPM2; TNNC1; TPM1; ATP2A2; ATP1B3; ATP1A1; PPP2R5C; ADRB2; ATP1B1; CACNB3; PPP2R2C; PPP2R3C; AKT2; CREB3L2; BCL2; GNAS; MAPK1; CALM2
Ribosome	22/170	1.10E-03	2.95E-02	−1.09	7.42	RPL4; RPL3; RPL21; RPL10; RPL12; RPS6; RPL11; MRPS10; RPL23A; MRPL36; MRPL23; MRPL12; RPL8; MRPL24; RPS15; RPS16; RPL27A; RPL37A; RPL14; RPL13; RPL18; RSL24D1
Enrichr pathway analysis: KEGG skNAC KD						
Term	Overlap	P-value	Adjusted P-value	Z-score	Combined Score	Genes
Alzheimer disease	24/175	2.93E-06	7.87E-04	−1.16	14.78	COX8A; GSK3B; NDUFB8; LRP1; APAF1; COX4I1; ATP5A1; COX7A2; IDE; GRIN2C; COX6A2; COX5A; PPP3CA; ADAM17; PLCB4; NDUFS6; GNAQ; ATP5D; MAPK1; UQCRC2; MAPT; NDUFV1; ATF6; SNCA
Insulin resistance	15/110	2.18E-04	2.21E-02	−1.74	14.65	GSK3B; MGEA5; NR1H2; GFPT2; PRKAG1; PYGM; PYGL; NFKB1; PPP1CA; MAPK10; CREB3; MAPK8; CREB3L2; MLX; SLC27A4
Non-alcoholic fatty liver disease (NAFLD)	18/151	3.02E-04	2.21E-02	−1.41	11.40	COX8A; GSK3B; NDUFB8; COX4I1; PRKAG1; COX7A2; ADIPOR1; COX6A2; COX5A; EIF2S1; NFKB1; MAPK10; ITCH; MAPK8; NDUFS6; MLX; UQCRC2; NDUFV1
Huntington disease	21/192	3.29E-04	2.21E-02	−1.14	9.15	COX8A; NDUFB8; GPX1; APAF1; COX4I1; DCTN4; ATP5A1; COX7A2; COX6A2; COX5A; SOD1; CREB3; PLCB4; NDUFS6; GNAQ; CREB3L2; ATP5D; VDAC3; VDAC2; UQCRC2; NDUFV1
Cardiac muscle contraction	11/78	1.10E-03	3.65E-02	−2.17	14.77	COX8A; SLC9A6; CACNA2D1; COX4I1; TNNC1; TPM1; COX7A2; ATP1A1; UQCRC2; COX6A2; COX5A
Hedgehog signaling pathway	8/44	9.72E-04	3.65E-02	−2.05	14.22	GSK3B; CCND2; CCND1; CSNK1A1; PTCH1; GAS1; ARRB2; CSNK1G2
Protein processing in endoplasmic reticulum	18/163	7.61E-4	3.65E-02	−1.51	10.82	SEC24A; FBXO2; DERL1; SYVN1; UBE2D1; UBE2J2; RAD23B; EIF2S1; CKAP4; MAPK10; DNAJC1; MAPK8; MAN1A2; DNAJC5; DNAJC10; UBQLN1; ATF6; CRYAB
Ubiquitin mediated proteolysis	16/138	8.67E-04	3.65E-02	−1.36	9.59	CUL7; MGRN1; FBXO2; SYVN1; XIAP; UBE2D1; UBE2J2; MID1; CUL4A; UBOX5; ITCH; CDC34; NEDD4; MDM2; ANAPC2; UBE2M
Parkinson disease	16/144	1.37E-03	3.65E-02	−1.25	8.24	COX8A; NDUFB8; APAF1; COX4I1; ATP5A1; COX7A2; UBE2J2; COX6A2; COX5A; NDUFS6; ATP5D; VDAC3; VDAC2; UQCRC2; NDUFV1; SNCA
Ribosome	18/170	1.24E-03	3.65E-02	−1.10	7.38	RPL4; RPL3; RPL21; RPL12; RPS6; MRPS10; RPL23A; MRPL36; MRPL12; MRPL24; RPS15; MRPL20; RPL14; RPL13; RPL27; RPL18; RPL29; RSL24D1
Human T-cell leukemia virus 1 infection	23/245	1.49E-03	3.65E-02	−0.82	5.36	FDPS; RANBP1; H2-DMA; XIAP; NFKB1; TGFBR2; MAPK10; PPP3CA; CREB3; KAT2A; MAPK8; CCND2; CCND1; CDK4; CREB3L2; VDAC3; VDAC2; MAPK1; B2M; MAP3K14; ANAPC2; JAK1; MAD2L1

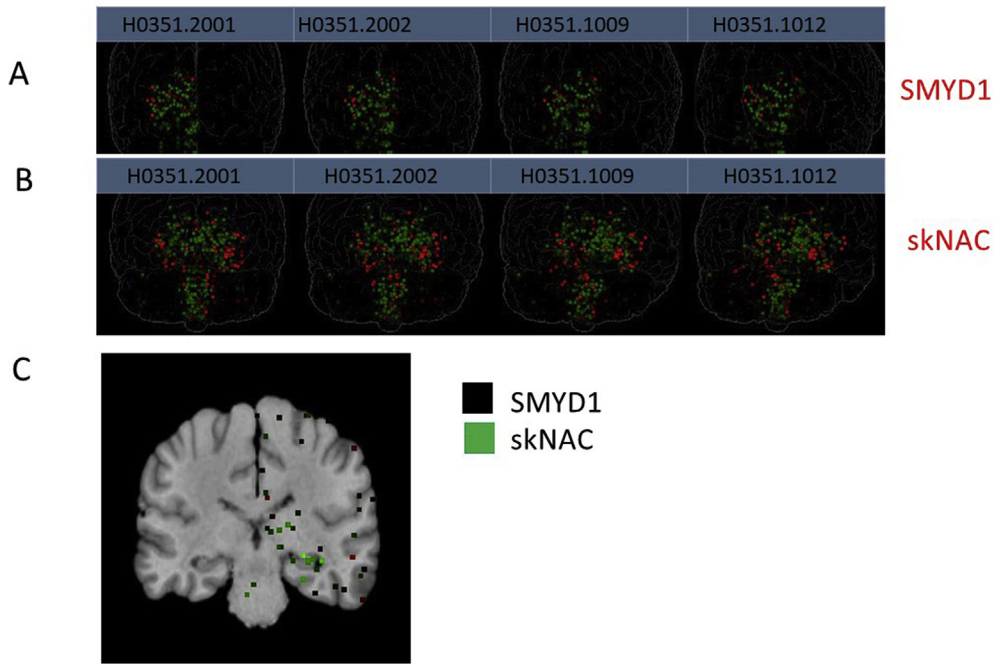

Fig. 2. Meta-analysis of human subcortical region accumulation of SMYD1 and skNAC. Images were downloaded and reformatted with permission from the Allen Mouse and Human Brain Atlases (Lein et al., 2007; Oh et al., 2014; Miller et al., 2017; Hawrylycz et al., 2012; Keller et al., 2018). Confidential patient identifiers (corresponding to images directly below) are indicated in blue boxes. **A, B**. Our meta-analyses of samples of normal human brains in which SMYD1 (A) or skNAC (B) RNA was identified by *in situ* RNA hybridization (red). Both accumulate primarily (but not exclusively; S-Fig. 3) within the subcortical striatum. **C.** RNA *in situ* detects expression of SMYD1 (red) and skNAC (green) within the striatum in near overlapping fashion.

detailed in Materials and Methods. Enriched protein fractions were fractionated on SDS-PAGE and subjected to anti-SMYD1 Western and anti-SMYD1 and anti-skNAC co-immunoprecipitation (co-IP) analyses.

As shown in Fig. 3A and B, we confirmed expression of SMYD1 and skNAC in the mouse cortex of each of the three TG subcortexes (TG-AD, TG-PD and TG-HD). We also confirmed low, and previously undetected, cortical transcripts in WT littermates of each of the above (Fig. 3C). Co-IPs of SMYD1 from subcortical lysates, following by probing for interaction with skNAC (Fig. 3D) revealed that SMYD1 and skNAC interact to varying extents within each. Reverse Co-IPs, employing anti-skNAC pulldowns probed with anti-SMYD1 Westerns blotting confirmed the interaction was reciprocal (Fig. 3E).

These data provided confidence that pursuit of additional, long-term studies in these mice models would be informative.

3.7. Differentiation of C2C12 myocytes into neurons

Our knockdown/gene array results summarized in Table 1 strongly implicated SMYD1 and skNAC in neuroinflammatory diseases. This was particularly unexpected, as our results were obtained from 3 day-

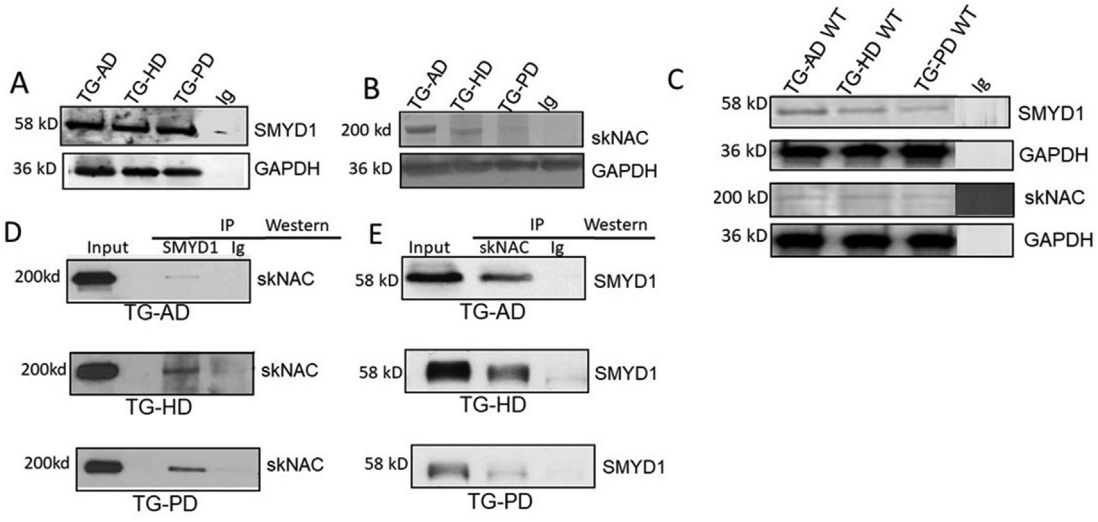

Fig. 3. SMYD1 and skNAC are expressed and associate within the murine subcortex of neuroinflammatory transgenic and wildtype transgenic mice. Subcortexes were prepared from 3 mouse transgenic (TG) models of Alzheimer's (TG^+-AD), Huntington's (TG^+-HD) and Parkinson's Diseases (TG^+-PD) (Goldberg et al., 2003; Pickrell et al., 2015; Konnova et al., 2018; Brüggemann et al., 2013) along with transgene negative (−) littermates. **A, B.** Representative Western blots (n = 4 independent experiments) of SMYD1 and skNAC in cultured subcortical neurons. Relatively strong bands are observed for each. **C.** Representative Western blot of each transgene WT (negative control). Weak expression was observed relative to TG^+ mice as judged by relative intensities of GAPDH. **D, E.** Reciprocal co-immunoprecipitation of SMYD1 inputs developed with anti-skNAC Western and skNAC inputs developed by anti-SMYD1 Western (n = 3 independent experiments) GAPDH served as a loading control; input controls (panels 1, 3); Ig, antibody-only negative controls (images taken at higher intensity so as to insure faint bands for TGs are not artifacts).

stimulated C2C12 myoblasts—not neurons. However, C2C12 myocytes are competent to differentiate into a number of cell lineages, including chondrocytes and osteoblasts, via addition of BMP4 (Chen et al., 2003), and into tenocytes, via addition of Myostatin/Chlorpromazine (MZ) (Ker et al., 2011; Uemura et al., 2017; Watanabe et al., 2004; Riazi et al., 2005). Notably in the present context, MZ, a member of the imidazole-based small molecule family, also was shown to promote neurogenesis in pluripotent stem cells (Kim et al., 2014).

Of the various conditions optimized for C2C12 cell neural differentiation (Chen et al., 2003; Ker et al., 2011; Uemura et al., 2017; Watanabe et al., 2004; Riazi et al., 2005; Kim et al., 2014), we chose successive incubation with MZ followed by incubation with Neuodazine (NZ), an antipsychotic medication primarily used to treat psychotic disorders such as schizophrenia (López-Muñoz et al., 2005).

Briefly, C2C12 myocytes, following 3 days of differentiation to myoblasts by serum withdrawal, were initially treated with MZ, which binds to microtubules and inhibits their conversion to angiogenesis by promoting mononucleates (Uemura et al., 2017; Watanabe et al., 2004). Note that even at this late myoblast differentiation stage, we began to detect what appeared to be dendritic-like cell body extensions (arrows in Fig. 4C. D). C2C12 mononucleates were then incubated with NZ for 6 more days. As shown in Fig. 4E–H, the NZ-treated mononucleates converted to a significant degree into neurogenic cells, as determined by phenotype and neuronal-specific staining (Materials and Methods). We observed that MZ/NZ treatment also converted satellite cells, obtained from mouse single muscle fibers, to neurons (data not shown).

We suspect that C2C12 myoblasts spontaneously underwent neural differentiation to a level sufficient to identify the neuroinflammatory-restricted targets of Table 1 and Fig. 1. Regardless, the data of Fig. 4 not only provided a rationale underlying why we detected immunoinflammatory SMYD1 and skNAC transcriptional targets but also a more simplified approach (below) toward confirming them.

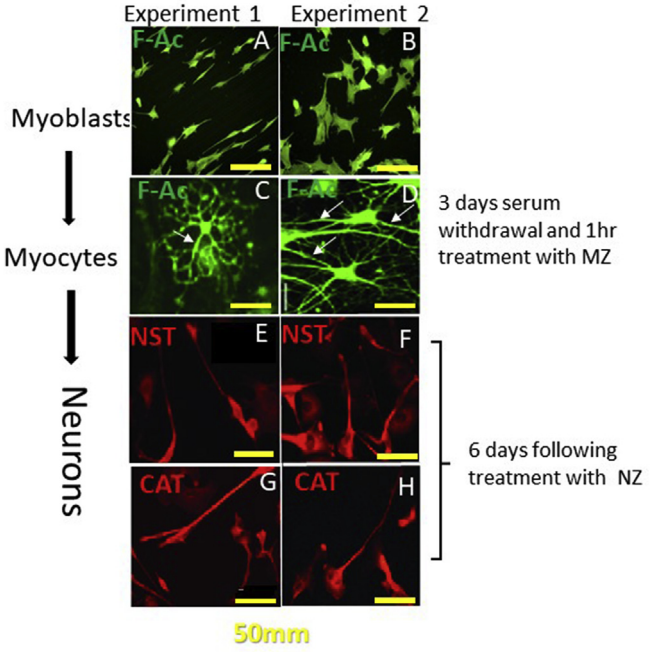

Fig. 4. Neurogenesis of C2C12 skeletal muscle myocytes. C2C12 myocytes (top row) were programmed to myoblasts (center row) via serum withdrawal/media change as previously described for 3 days (Sims et al., 2002). Myoblasts were treated with Myoseverin (MZ) for 1 day and then with Chlorpromazine (Neurazine, NZ) for 6 days as indicated by the schematic and detailed in Materials and Methods. Cell types were identified by morphology and by staining with FITS-phalloidin to identify F-Actin (F-Ac, green) or with neuronal antibodies (red) to identify neuron-specific tubulin (NST) and choline acetyltransferase (CAT) positive neurons. Scale bars = 50 mm (yellow). Shown are two representative images (Experiment 1 and Experiment 2) representative of 5 independent experiments. (For interpretation of the references to color in this figure legend, the reader is referred to the Web version of this article.)

3.8. SMYD1, but not skNAC is required for C2C12 neuron reprogramming

We employed SMYD1-and skNAC sh-RNAs to determine if either SMYD1, skNAC or both were essential for reprogramming C2C12 myoblasts to neurons. C2C12 myocytes were infected with either SMYD1-or skNAC sh-RNA, cultured 3 days to form myoblasts, and then cultured with MZ and NZ under the neurogenesis protocol described above and in Materials and Methods.

As shown in Fig. 5A, we detected a clear reduction in acquisition of neuronal phenotype following SMYD1 sh-RNA KD, but no observable change was observed following skNAC KD relative to mock-transduced C2C12 controls.

To quantify the reduction in SMYD1- and skNAC-silenced cells, we employed three-dimensional reconstructions using Neurolucida software (Peng et al., 2015) and detailed in S-Methods) of each mouse reprogrammed neuron that displayed the parameters of somato-dendritic morphology. Shown in Fig. 5B are typical examples calculated from a minimum of 180 dendrites imaged. The majority of the control and skNAC-depleted spiny neurons (Fig. 5Da, c) had medium sized soma and

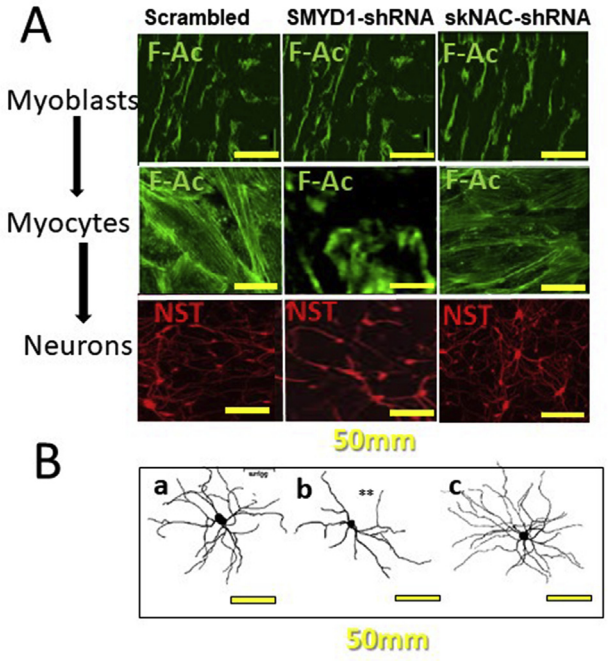

Fig. 5. SMYD1, but not skNAC retards neurogenesis of reprogrammed C2C12 neurons. A. C2C12 myoblasts were infected with retroviral shRNAs encoding either a scrambled sequence (left lanes), a sequence specific for SMYD1 (center lanes) or specific for skNAC (right lanes) prior to 3 days differential of C2C12 myocytes to myoblasts. On day 3, MZ was added at day 3 followed 1 h later with NZ addition for 6 days and then neuron differentiation was assessed morphology or with neuron-specific stains as described in the legend of Fig. 4. Scale bars = 50 mm (yellow). **B.** Quantification of SMYD1 and skNAC-silenced neuronal differentiation by three-dimensional reconstructions of reprogrammed neurons of somato-dendritic morphologically using Neurolucida software (59 and detailed in S-Methods). Shown are typical examples calculated from a minimum of 180 dendrites imaged. SMYD1 sh-RNA treated neurons in Fig. 5Bb had significantly lower density as determined by one-way analysis of variance (Uylings et al., 1989) ($p \leq 0.01$; indicated by **). Scale bars (yellow) = 50 mm. Results and statistics calculated from 5 independent experiments. (For interpretation of the references to color in this figure legend, the reader is referred to the Web version of this article.)

spine-laden dendrites. Their density increased gradually towards distal segments, with some showing numerous collateral branches. However, in SMYD1 sh-RNA treated neurons (Fig. 5Db), the somato-dendritic pattern, while still observed, had significantly lower density in relation to their size of their cell bodies. A statistically significant difference ($p \leq 0.01$) between scrambled control and SMYD KD was determined by one-way analysis of variance (Uylings et al., 1989).

These data indicated that SMYD1 is the rate-limiting factor—at least in this *in culturo* format of myoblasts to neuronal differentiation.

3.9. Transcripts associated with neuroinflammatory diseases are deregulated by SMYD1 and/or skNAC loss in reprogrammed C2C12 neurons

We preformed RT-qPCR of RNA isolated from reprogrammed skNAC-shRNA or SMYD1-shRNA transduced C2C12 neurons in an attempt to confirm and quantify expression of selective neurodegenerative transcripts identified by expression arrays (see Fig. 1). We analyzed the data according to either singular loss of SMYD1 or skNAC as well as dual loss of both. Scrambled sequences of SMYD1 or skNAC sh-RNAs served as controls (CNTR); oligonucleotide primers employed for RT-qPCR are listed in Table 2.

As shown in Fig. 6A, SMYD1 KD of transcripts determined in Table 1 detected 13 unique targets with 9 of these confirmed by RT-qPCR (Fig. 6A). skNAC KD yielded 7 unique targets with 4 confirmed (Fig. 6B, left panel). Note that the magnitude of fold change mediated by skNAC KD was almost a log lower than that achieved by SMYD1 KD, with the exception of ADAM17 (6 B, right panel). These data support the observations of Fig. 5 and further suggested that the dominant factor in the system is SMYD1.

There were 7 transcripts with 5 statistically deregulated by both SMYD1 and skNAC (Fig. 6C). In Fig. 6D, we observed 5 deregulated transcripts which are particularly relevant to AD. As anticipated from the data of Table 1, NDUF, COX and ATPase transcripts dominated each of the C2C12 neuronal categories. The large number of transcripts co-regulated by SMYD1 and skNAC suggest that, while SMYD1 may rate limiting, SMYD1 and skNAC might be functioning as heterodimers, at least in most of the cases.

The results are discussed below in the context of neuroinflammation and are illuminated in the AD pathway of S-Fig. 4.

Table 2
Oligonucleotide primers for genes targeted by SMYD1, skNAC or both. Sequences designed to amplify the junction between two exons using the primer 3 program with NCBI reference sequences (right).

GENE	OLIGONUCLEOTIDE PRIMERS		ACCESSION #
	Forward	Reverse	
SMYD1 KD			
NDUFB11	CCTATCTGCCTGACTACAGGTG	GGTCGAAGCAGTTGGATTCCATG	NM_001135998
COX7B	CACCAGAAGAGGGCACCTAGTT	TGACTCTGCCAACAGGGGACAT	NM_025379
ATP5A1	GCACGGGCTGAGGAATGT	CCAACAGCTCCTCGCCAA	NM_007505.2
NDUFA10	CCAGGAATCGTACACCAACACC	GAAGGTACCTCTGCCTATCTC	NM_024197
NDUFAF8	GTACGGCAGGTGCGTGCAGG	AGCCTCCCTCCAGCGTCTTCT	NM_001086521
ATPQA1	ATTCACCCTGGAGTTCTCCCGA	CTCGCACATAGTTACAGCGGTC	NM_001286075
COX5A	CAGATGAGGAGTTTGATGCTCGC	GCAGCATCAATGATTTTGGGCTC	NM_004255
ATP5H	GCCTTCCAGGACGGGACTCCAT	GTCCGTGGAGATTCGACCCAACAC	NM_008084
COX7A2	TCACGAAGGCATTTTGAAAACA	CCCCGCCTTTCAGATGAAC	NM_001865.3
ATP5G3	TTCTGCATCAGTGTTATCTCGG	ATGCCAACATTTCAGGCAGTA	NM_175015.1
ATP5D	GTAGGAGTTGCTGGTTCTGGTG	GCTTCAGACAAGGCAAATCCCAG	NM_001301721
COX6A2	GCTCCCTTAACTGCTGGATGCA	TGGAAAAGCGTGTGGTTGCCGT	NM_009943
UQCRC2	CCGTGGAATTGAAGCAGTTGGTG	CTGTGGTGACATTGAGCAGGAAC	NM_003366
skNAC KD			
NDUF56	TGGAGACTCGGGTGATAGCGTG	GTGGTGCTGTCTGAACTGGAGC	NM_004553
COX8A	AACTTCCGGCTGGCCATCTTGAC	AGCCGCCGGGCCGGAGCCGGTC	NM_007750
NDUFS2	CCAATTCGCGCACAGTGGA	CCTGGTCGACGTATGCAGC	NM_004550
APAF1	GCCAAGCAGGAGGTCGATAATG	GACCATCCTCAGAAAAGCAGGC	NM_001160
ADUFV1	TGTGTGAGACGGTGCTGATGGA	CGATGGCTTTCACGATGTCCGT	NM_001166102
SMYD1 + skNAC KD			
COX4I1	TCATTGGCTTCACTGCGCTCGT	TCCAGCATTCGCTTGGTCGCA	NM_009941
COX5A	CAGATGAGGAGTTTGATGCTCGC	GCAGCATCAATGATTTTGGGCTC	NM_004255
ATP5D	ACTGGAGCCTTTGGCATCTTGG	AGTCGGCATTCACAGTGACGGA	NM_001347092
ATF6	GTCCAAAGCGAAGAGCTGTCTG	AGAGATGCCTCCTCTGATTGGC	NM_001081304
COX7A2	CGAAGGACATTTTGAAAACAAGGTTC	ACCAAGCGTCGAGCCATTGTG	NM_009945
ATP8IPK	ACGCCTTTGACGGTGCCGATTA	AAGTCGCTGATGGCTTTCCTGG	BC013766
KCHIP3	GCATACCACTGAGCAAGAGGGA	TGATGGCGACCGTGGATAACT	NM_001291005
Neuroinflammation			
ATF6	GTCCAAAGCGAAGAGCTGTCTG	AGAGATGCCTCCTCTGATTGGC	NM_001081304
COX7A2	CGAAGGCATTTTGAAAACAAGGTTC	ACCAAGCGTCAGAGCCATTGTG	NM_009945
ATPS8IPK	ACGCCTTTGACGGTGCCGATTA	AAGTCGCTGATGGTTTCCTGG	BC013766
KCHIP3	GCATACCACTGAGCAAGAGGGA	TGATGGCGCACCGTGGATAACT	NM_001291005
ATPSD	CGGAGCCTTCGGCATCCTGG	AGAGTCGGCGTTCACTGCGAT	NM_001001975
SNCA	CACTGGCTTTGTCAAGAAGGACC	CATAAGCCTCACTGCCAGGATC	NM_009221
ATP5D	ACTGGAGCCTTTGGCATCTTGG	AGTCGGCATTCACAGTGACGGA	NM_001347092
UQCRC2	ATGCCACCTTCTACCGTCCTTC	GTTTCCACTCGCTGCCATTGAC	NM_025899
MAP1	CCTGAGCAAAGTGACCTCCAAG	CAAGGAGCCAATCTTCGACTGG	NM_001038609
Controls			
GAPDH	CATCACTGCCACCCAGAAGACTG	ATGCCAGTGAGCTTCCCGTTCAG	NM_001289726
ACTB	CATTGCTGACAGGATGCAGAAGG	TGCTGGAAGGTGGACAGTGAGG	NM_007393

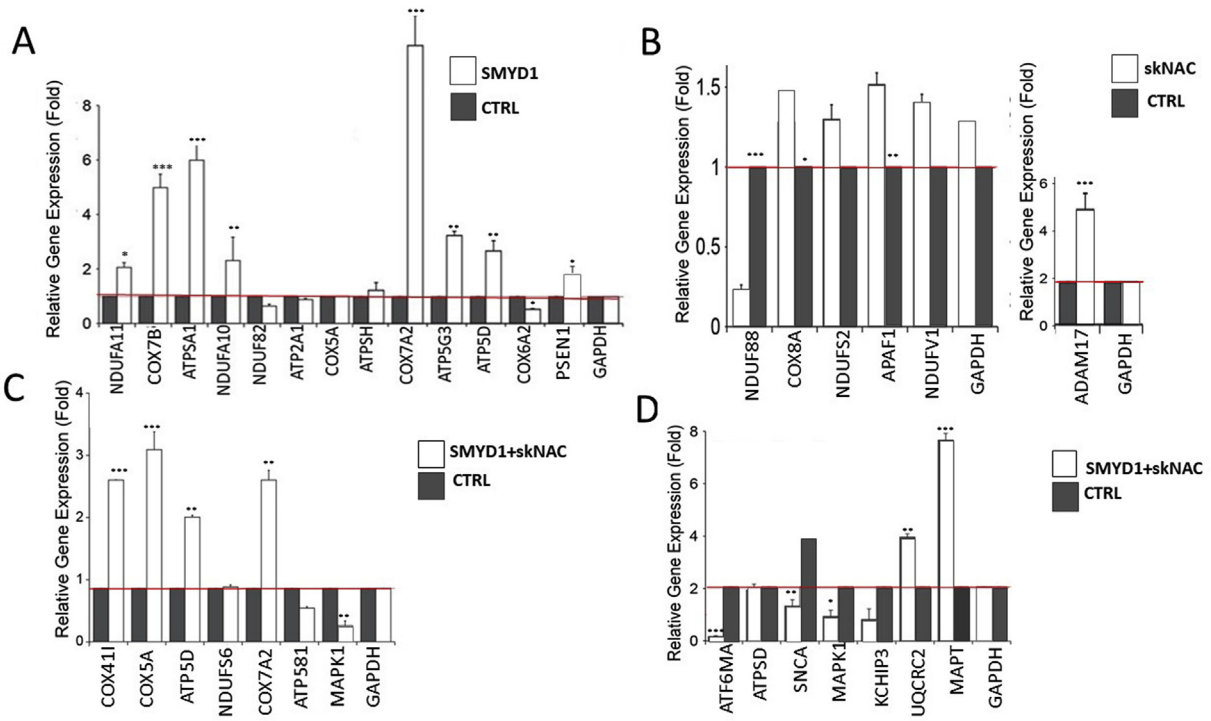

Fig. 6. Key neuroinflammatory molecules are deregulated by SMYD1 and/or skNAC loss in reprogrammed C2C12 neurons. Total RNA was isolated from cultured C2C12 differentiated neurons following sh-RNA KD of either SMYD1 or skNAC as detailed in Fig. 4 and S-Methods. RT-qPCR primers were designed to amplify the junction between two exons using the primer 3 program (Table 2). CT values were normalized to 1 against GAPDH. Shown are results of at least 4 independent measurements; *, $p \leq 0.05$; **, $p \leq 0.01$; ***, $p \leq 0.01$ as determined by students T-tests. **A.** SMYD1 KD detected 13 unique targets with 9 of these confirmed. **B.** skNAC KD yielded 13 unique targets with 4 statistically confirmed. Note: Their magnitudes are ~1 log lower than in other panels with the exception of ADAM17 (right panel). **C.** SMYD1 and skNAC shared 7 targets with 5 statistically altered. **D.** Deregulated factors that play key roles in AD, and to a lesser extent, HD and PD pathology. These include 5 targets confirmed as deregulated following KD of both SMYD1 and skNAC. Targets are identified in the KEGG Alzheimer's Disease Pathways of S-Fig. 4.

3.10. SMYD1 and/or skNAC regulate factors central to neuroinflammation including Tau

Foremost among this group is Microtubule-Associated Protein Tau (MAPT). Tau/MAPT transcripts undergo complex and highly regulated alternative splicing. This leads to their differential expression in the nervous system, depending on stage of neuronal maturation and neuron type (Strang et al., 2019; Caillet-Boudin et al., 2015). *Mapt* mutations are associated with several neurodegenerative disorders, particularly Alzheimer's (Smyth, Grosser et al., 2820; Lezi and Swerdlow, 2012; Canu-Sarasso et al., 2018; JT O'Brien et al., 2017; Bray, 2020; Elkouzi, Vedam-Mai et al., 2019). While the normal function of Tau is to organize microtubules, in Alzheimer's Tau collapses into tangled aggregates termed "Tau's tangles". Brain alterations result via a complex interplay among abnormal Tau, beta-amyloid proteins and several other factors (Smyth, Grosser et al., 2820; Lezi and Swerdlow, 2012; CanuSarasso et al., 2018; JT O'Brien et al., 2017; Bray, 2020; Elkouzi, Vedam-Mai et al., 2019).

The consequence of Tau neurofibrillary tangles leads to "senile plaques" composed of extracellular deposits of aggregated Amyloid-beta protein (A-beta)—the proposed causative agent of AD (Strang et al., 2019; Caillet-Boudin et al., 2015). A-beta is enzymatically processed to Amyloid Precursor Protein (APP) primarily via several alpha-secretases, including the skNAC target ADAM17 (Fig. 6B**).**

AD patients with a genetically inherited form of the disease have mutations in APP or in Presenilin proteins (Bekris et al., 2010). These include PSEN1, a target of SMYD1 repression (Fig. 6A). PSENs regulate APP processing via their cleavage of several gamma-secretases. MAPK1/ERK kinase, repressed by both SMYD1 and skNAC (Fig. 6C), promotes formation of autophagosome vesicles that contain A-beta as well as gamma secretases also required to generate APP (Li et al., 2019).

ATF6 encodes a transcription factor (repressed by SMYD1 and skNAC; Fig. 6D) that activates target genes required for the unfolded protein response during endoplasmic reticulum (ER) stress (López-Hurtado et al., 2018). Immunohistochemical studies revealed that neurons in postmortem brain samples of AD patients display prominent expression of markers of ER stress (López-Hurtado et al., 2018). ATF6 also is deregulated in HD and PD (Colla, 2019; Talya et al., 2019). Dual SMYD1 + skNAC downregulation of KCHIP3 is particularly interesting in this regard. KCHIP3/DREAM is part of an endogenous neuroprotective mechanism that interacts with and accelerates ATF6 processing as well as neuronal survival in the striatum of R6/2 mice (Li et al., 2019)—a model of HD (Konnova et al., 2018).

3.11. Key aging factors underlying neurodegeneration are deregulated by SMYD1 and/or skNAC loss

Aging is the strongest risk factor for neurodegenerative diseases including (reviewed in Thies and Bleiler, 2011). Aging is accompanied by increased mitochondrial reactive oxygen species whose dysregulation damages mtDNA and/or mitochondrial components (Thies and Bleiler, 2011). Numerous mechanisms have implicated mitochondria in aging and in multiple neurodegenerative diseases, including AD, PD, and HD (Lezi and Swerdlow, 2012; Colla, 2019; Talya et al., 2019; Thies and Bleiler, 2011).

Most of the ATP of a cell is produced through oxidative phosphorylation (OXPHOS) in mitochondria driven by the electron transport chain composed of 4 respiratory complexes (CXI, CX2, CX3, and CXIV) (reviewed in Berg et al., 2002). SMYD1 and skNAC loss deregulate primarily component polypeptides within CX-I (NDUFA11, NDUFA10 and

ATPG3) and CX-IV (COX7B, COX5A, ATPD5 and COX7A2) (Fig. 6A–D, S-Fig. 4). Deregulation of both of these enzyme complexes have been implicated in AD, PD and HD (CanuSarasso et al., 2018; JT O'Brien et al., 2017; Bray, 2020; ElkouziVedam-Mai et al., 2019; GiauSenanarong et al., 2019; Berg et al., 2002). Previous studies also have correlated disruption of CX-I and IV with Aβ plaque burden in the hippocampi of AD TF mice (Goldberg et al., 2003; Pickrell et al., 2015).

Mitochondrial dysfunction, because of its critical role in energy production and cellular metabolism, is a strongly implicated susceptibility factor for AD, PD and HD (Lezi and Swerdlow, 2012; Canu, Sarasso et al., 2018). SMYD1 and skNAC modulated expression of a family of Cyclooxygenase (COX) isoforms (Fig. 6C, S-Fig. 4, which are required both for the formation of prostanoids (including prostaglandins) (Smyth, Grosser et al., 2820) as well as for modulation of NDUFA isoforms—a complex within the mitochondrial electron transport chain (Lezi and Swerdlow, 2012). UQCRC2/CX3, also repressed by both SMYD1 and skNAC, localizes to the mitochondrion, where as part of the ubiquinol-cytochrome c reductase complex (CX-III), it is required for mitochondrial OXPHOS (Berg et al., 2002). UQCRC2 and additional components of CX-III are down-regulated in early onset AD as well as in HD and PD (Adav et al., 2019).

Finally, oxidative phosphorylation and glycolysis are metabolically linked, as pyruvate is transferred to the mitochondria to produce energy precursors of OXPHOS. (Berg et al., 2002). Evidence indicates that glucose metabolism is disrupted in AD brains (Calsolaro and Edison, 2016). Several molecular markers of glycometabolism, including the SMYD1 and skNAC target, ATP5D (Fig.6C; S-Fig. 4), are downregulated in AD and other neuroinflammatory diseases (Ding et al., 2014; Sprenkle et al., 2017).

4. Discussion

Synaptic dysfunction in Alzheimer's, Parkinson's and Huntington's disease is largely caused by failed protein homeostasis, because defective, unfolded proteins accumulate pathogenic protein aggregates at synapses (Herms and Dorostkar, 2016). Gene deregulation underlying several transcripts that direct or carry out these devastating consequences have been observed in the present analyses of two, previously unanticipated players—SMYD1 and skNAC.

While the data presented here must be considered preliminary, they strongly suggest that the use of reprogrammed C2C12 neurons can be informative in deducing/confirming proteins downstream of SMYD1 and skNAC involved in neuroinflammation. We currently are utilizing both the neuroinflammatory mouse models of Fig. 3, as well as diseased human brain tissues from the Alzheimer's Disease Center at University of Texas Southwestern Medical Center to carry out direct tests of the hypotheses generated in this report.

Histone methylation generally is associated with transcriptional repression (Tracy et al., 2018). SMYD1 has been shown to catalyze tri-methylation of histones H3Km3, H3K9m1 and potentially additional, but as yet uncharacterized, histone methylation marks (Tracy et al., 2018; Paik and Zon, 2010). There are two exceptions: Tribbles3 and skNAC. When directly methylated by SMYD1, Tribbles3 is activated to act as a co-repressor of SMYD1-mediated transcription during oxidative stress (Nie et al., 2017). We also showed recently that SMYD1 methylation of skNAC is required for its full transcriptional activation of Myoglobin (C. Li et al. submitted).

In this report, we observed that only 5 of 28 SMYD1 or SMYD1/skNAC dual targets were activated. This strongly indicated that the repressive role of histone or non-histone modification, as well as the more conventional transcriptional repression documented for both SMYD1 and skNAC (Yahalom et al., 2018; Tracy et al., 2018; Franklin et al., 2016; Murayama et al., 2015; Rasmussen et al., 2015; Rasmussen and Tucker, 2018; Fujii et al., 2016; Hsia and Zon, 2005), are essential features for future exploration. To comprehensively address this issue, we plan to carry out global transcriptional analyses, including Chip-seq of both human and mouse genomes following SMYD1 and skNAC loss, using approaches we have performed previously for a number of TFs (Dekker et al., 2016, 2019; Kim et al., 2016b; Ippolito et al., 2014). We also plan to determine the methylation status catalyzed by SMYD1 HMTase activity that may supplement the transcriptional regulation determined here using methods we have employed previously (Rhee et al., 2014; An et al., 2010). Results of these experiments will be critical in providing a full mechanistic account of the role of SMYD1 and skNAC in neuroinflammatory disease.

Finally, we submit that ultimately the data here, coupled with the above approaches, may render SMYD1, or a small molecule mimic, an excellent clinical biomarker of neurodegenerative diseases.

Author contributions

RDM and HOT designed research; LZ, TAS, and GRT performed research; RDM, LZ, RDM, GRT and HOT analyzed data; RDM and HOT wrote the manuscript.

Declaration of competing interest

The authors declare no competing financial interests.

Acknowledgements

We thank the late Dr. Paul Gottlieb for his discovery of SMYD1 and initiating this project. We thank June Harriss, Debora Lerner and the late, Shan Mika for their excellent contribution to all aspects of the animal husbandry. We thank Chhaya Das and Maya Ghosh for help in cell culture and molecular techniques. We thank members of the Tucker laboratory for discussions and reading of the manuscript. We were provided extensive experimental support at the MD Anderson Smithville Core Facilities, directed by Dr. J.J. from the following employees: Luis Coletta, Melissa Simper, Yueping Chen, Yoko Takata and Carol Mikulec. H.O.T. received support for this work from NIH Grant R01CA31534, Cancer Prevention Research Institute of Texas (CPRIT) Grants RP100612, RP120348; and the Marie Betzner Morrow Centennial Endowment. NIH/NIAAA Grant U01 AA020926 (RDM).

Appendix A. Supplementary data

Supplementary data to this article can be found online at https://doi.org/10.1016/j.bbih.2020.100129%20.

References

Adav, S.S., Park, J.E., Sze, S.K., 2019. Quantitative profiling brain proteomes revealed mitochondrial dysfunction in Alzheimer's disease. Mol. Brain 12, 8. https://doi.org/10.1186/s13041-019-0430-y.

Alzheimer's Association Report, 2019. Alzheimer's Dementia 15 (3), 321–387.

Thies, W., Bleiler, L., 2011. Alzheimer's disease facts and figures. Alzheimer's Dementia 7 (2), 208–244, 2011.

An, G., Miner, C.A., Nixon, J.C., Kincade, P.W., Bryant, J., Webb, C.F., Tucker, H.O., 2010. Loss of Bright/ARID3a function promotes developmental plasticity. Stem Cell. 28 (9), 1560–1567. https://doi.org/10.1002/stem.491.

Arendt, T., Brückner, M.K., Morawski, M., et al., 2018. Early neurone loss in Alzheimer's disease: cortical or subcortical? Acta neuropathol. Commun. 3 (10), 34–43.

Bekris, L.M., Yu, C.E., Bird, T.D., Tsuang, D.W., 2010. Genetics of alzheimer disease. J. Geriatr. Psychiatr. Neurol. 23 (4), 213–227. https://doi.org/10.1177/0891988710383571.

Berg, J.M., Tymoczko, J.L., Stryer, L., 2002. Biochemistry, fifth ed. W H Freeman, New York. Section 18.3, The Respiratory Chain Consists of Four Complexes: Three Proton Pumps and a Physical Link to the Citric Acid Cycle. https://www.ncbi.nlm.nih.gov/books/NBK22505/.

Bray, N., 2020. Hunting out mutant Huntingtin. Nat. Rev. Neurosci. 21, 3. https://doi.org/10.1038/s41583-019-0248-8.

Brüggemann, N., Klein, C., 2013. Parkin type of early-onset Parkinson Disease. In: Adam, M.P., Ardinger, H.H., Pagon, R.A., et al. (Eds.), GeneReviews. Seattle (WA). https://www.ncbi.nlm.nih.Gov/books/NBK1478/.

Caillet-Boudin, M., Buée, L., Sergeant, N., et al., 2015. Regulation of human MAPT gene expression. Mol. Neurodegener. 10, 28.

Calsolaro, V., Edison, P., 2016. Alterations in glucose metabolism in Alzheimer's disease. Recent Pat. Endocr. Metab. Immune Drug Discov. 10 (1), 31–39.
Canu, E., Sarasso, E., Filippi, M., et al., 2018. Effects of pharmacological and nonpharmacological treatments on brain functional magnetic resonance imaging in Alzheimer's disease and mild cognitive impairment: a critical review. Alz Res Therapy 10, 21. https://doi.org/10.1186/s13195-018-0347-1.
Chen, Y., Luk, K.D., Cheung, K.M., Xu, R., Lin, M.C., Lu, W.W., Leong, J.C., Kung, H.F., 2003. Gene therapy for new bone formation using adeno-associated viral bone morphogenetic protein-2 vectors. Gene Ther. 10, 1345–1353.
Chen, E.Y., et al., 2013. Enrichr: interactive and collaborative HTML5 gene list enrichment analysis tool. BMC Bioinf. 14, 128.
Colla, E., 2019. Linking the endoplasmic reticulum to Parkinson's Disease and alpha-synucleinopathy. Front. Neurosci. 13, 560. https://doi.org/10.3389/fnins.2019.00560.
Dekker, J.D., Park, D., Shaffer 3rd, A.L., Kohlhammer, H., Deng, W., Lee, B.K., Ippolito, G.C., Georgiou, G., Iyer, V.R., Staudt, L.M., Tucker, H.O., 2016. Subtype-specific addiction of the activated B-cell subset of diffuse large B-cell lymphoma to FOXP1. Proc Natl Acad Sci U S A. 2 113 (5), E577–E586. https://doi.org/10.1073/pnas.1524677113.
Dekker, J.D., Baracho, G.V., Zhu, Z., et al., 2019. Loss of the FOXP1 transcription factor leads to deregulation of B lymphocyte development and function at multiple stages. Immunohorizons 3 (10), 447–462. https://doi.org/10.4049/immunohorizons.1800079.
Ding, B., Xi, Y., Gao, M., Li, Z., Xu, C., Fan, S., He, W., 2014. Gene expression profiles of entorhinal cortex in Alzheimer's disease. Am. J. Alzheimer's Dis. Other Dementias 6, 526–532.
Elkouzi, A., Vedam-Mai, V., Eisinger, R.S., et al., 2019. Emerging therapies in Parkinson disease- repurposed drugs and new approaches. Nat. Rev. Neurol. 15, 204–223. https://doi.org/10.1038/s41582-019-0155-7.
Franklin, S., et al., 2016. The chromatin-binding protein Smyd1 restricts adult mammalian heart growth. Am. J. Physiol. Heart Circ. Physiol. 311, H1234–H1247.
Fujii, T., Tsunesumi, S., Sagara, H., et al., 2016. Smyd plays pivotal roles in both primitive and definitive hematopoiesis during zebrafish embryogenesis. Sci. Rep. 6, 29157.
Giau, V.V., Senanarong, V., Bagyinszky, E., An, S.S.A., Kim, S., 2019. Analysis of 50 neurodegenerative genes in clinically diagnosed early-onset Alzheimer's Disease. Int. J. Mol. Sci. 20 (6), 1514. https://doi.org/10.3390/ijms20061514.
Goldberg, M.S., Fleming, S.M., Palacino, J.J., Cepeda, C., Lam, H.A., Bhatnagar, A., Meloni, E.G., Wu, N., Ackerson, L.C., Klapstein, G.J., Gajendiran, M., Roth, B.L., Chesselet, M.F., Maidment, N.T., Levine, M.S., Shen, J., 2003. Parkin-deficient mice exhibit nigrostriatal deficits but not loss of dopaminergic neurons. J. Biol. Chem. 278 (44), 43628–43635.
Gupta, Y., Lee, K.H., Choi, K.Y., Lee, J.J., Kim, B.C., Kwon, G.-R., 2019. Alzheimer's Disease diagnosis based on cortical and subcortical features. J.Healthcare Engineer 1–13.
Hawrylycz, M.J., et al., 2012. An anatomically comprehensive atlas of the adult human transcriptome. Nature 489, 391–399.
Herms, J., Dorostkar, M.M., 2016. Dendritic spine pathology in neurodegenerative diseases. Annu. Rev. Pathol. 11, 221–250.
Holper, L., Ben-Shachar, D., Mann, J.J., 2019. Multivariate meta-analyses of mitochondrial complex I and IV in major depressive disorder, bipolar disorder, schizophrenia, Alzheimer disease, and Parkinson disease. Neuropsychopharmacology 44 (5), 837–849.
Hsia, N., Zon, L.I., 2005. Transcriptional regulation of hematopoietic stem cell development in zebrafish. Exp. Hematol. 33, 1007–1014.
Ippolito, G.C., Dekker, J.D., Wang, Y.H., Lee, B.K., Shaffer 3rd, A.L., Lin, J., Wall, J.K., Lee, B.S., Staudt, L.M., Liu, Y.J., Iyer, V.R., 2014. Tucker HO Dendritic cell fate is determined by BCL11A. Proc. Natl. Acad. Sci. U. S. A. 111 (11), E998–E1006. https://doi.org/10.1073/pnas.1319228111.
Jankowsky, J.L., Fadale, D.J., Anderson, J., Xu, G.M., Gonzales, V., Jenkins, N.A., Copeland, N.G., Lee, M.K., Younkin, L.H., Wagner, S.L., Younkin, S.G., Borchelt, D.R., 2004. Mutant presenilins specifically elevate the levels of the 42 residue beta-amyloid peptide in vivo: evidence for augmentation of a 42-specific gamma secretase. Hum. Mol. Genet. 13 (2), 159–170.
Jing, L., Zon, L.I., 2011. Zebrafish as a model for normal and malignant hematopoiesis. Dis Model Mech 4, 433–438.
JT O'Brien, J.T., Holmes, C., Jones, M., Jones, R., Livingston, G., McKeith, I., et al., 2017. Clinical practice with anti-dementia drugs: a revised (third) consensus statement from the British Association for Psychopharmacology. J. Psychopharmacol. 31, 147–168.
Kanehisa, M., Sato, Y., Kawashima, M., Furumichi, M., Tanabe, M., 2016. KEGG as a reference resource for gene and protein annotation. Nucleic Acids Res. 44, D457–D462.
Keller, D., Erö, C., Markram, H., 2018. Cell Densities in the mouse brain: a systematic review. Front. Neuroanat. 12, 83–90. https://doi.org/10.3389/fnana.2018.00083.
Ker, E.D., Nain, A.S., Weiss, L.E., Wang, J., Suhan, J., Amon, C.H., Campbell, P.G., 2011. Bioprinting of growth factors onto aligned sub-micron fibrous scaffolds for simultaneous control of cell differentiation and alignment. Biomaterials 32, 8097–8107.
Kim, G.-H., Halder, D., Park, J., Nambung, W., Shin, I., 2014. KiImidazole-based small molecules that promote neurogenesis in pluripotent cells. Angew. Chem. 126 (35), 9425–9428.
Kim, J.Y., Lee, J.H., Sun, W., 2016a. Isolation and culture of adult neural stem cells from the mouse subcallosal zone. JoVE 118, e54929. https://doi.org/10.3791/54929.
Kim, P.G., Canver, M.C., Rhee, C., Ross, S.J., Harriss, J.V., Tu, H.C., Orkin, S.H., Tucker, H.O., Daley, G.Q., 2016b. Interferon-α signaling promotes embryonic HSC maturation. Blood 128 (2), 204–216. https://doi.org/10.1182/blood-2016-01-689281.
Konnova, E.A., Swanberg, M., 2018. Animal models of Parkinson's disease. In: Stoker, T.B., Greenland, J.C. (Eds.), Parkinson's Disease: Pathogenesis and Clinical Aspects. Codon Publications, Brisbane (AU) (Chapter 5).
Kuleshov, M.V., et al., 2016. Enrichr: a comprehensive gene set enrichment analysis web server 2016 update. Nucleic Acids Res. 44, W90–W97.
Lein, E.S., et al., 2007. Genome-wide atlas of gene expression in the adult mouse brain. Nature 445, 168–176.
Lezi, E., Swerdlow, R.H., 2012. Mitochondria in neurodegeneration. Adv. Exp. Med. Biol. 942, 269–286. https://doi.org/10.1007/978-94-007-2869-1_1221.
Li, Q., Wang, Y., Peng, W., et al., 2019. MicroRNA-101a regulates autophagy phenomenon via the MAPK pathway to modulate alzheimer's-associated pathogenesis. Cell Transplant. 28 (8), 1076–1084.
López-Hurtado, A., Burgos, D.F., González, P., et al., 2018. Inhibition of DREAM-ATF6 interaction delays onset of cognition deficit in a mouse model of Huntington's disease. Mol. Brain 11 (1), 13–22, 2018.
López-Muñoz, F., et al., 2005. History of the discovery and clinical introduction of chlorpromazine. Ann. Clin. Psychiatr. (3), 113–135. https://doi.org/10.1080/1040123059100.
Maiti, P., Manna, J., Dunbar, G.L., 2018. Current understanding of the molecular mechanisms in Parkinson's disease: targets for potential treatments. Transl. Neurodegener. 6, 28. https://doi.org/10.1186/s40035-017-0099-z.
Meeson, A.P., et al., 2001. Adaptive mechanisms that preserve cardiac function in mice without myoglobin. Circ. Res. 88, 713–720.
Miller, J.A., et al., 2017. Neuropathological and transcriptomic characteristics of the aged brain. Elife 6. https://doi.org/10.7554/eLife.31126.
Murayama, E., Sarris, M., Redd, M., et al., 2015. NACA deficiency reveals the crucial role of somite-derived stromal cells in haematopoietic niche formation. Nat. Commun. 6, 8375.
Myers, A., McGonigle, P., 2019. Overview of transgenic mouse models for Alzheimer's disease. Curr Protoc Neurosci 89 (1), e81. https://doi.org/10.1002/cpns.81.
Nie, H., Rathbun, G., Tucker, H., 2017. Smyd1C mediates CD8 T cell death via regulation of Bcl2-mediated restriction of outer mitochondrial membrane Integrity. J Cell Signal 2 (3), 163–170, 2.
Oh, S.W., et al., 2014. A mesoscale connectome of the mouse brain. Nature 508, 207-21439.
Paik, E.J., Zon, L.I., 2010. Hematopoietic development in the zebrafish. J. Dev. Biol. 5, 1127–1137.
Park, C.Y., et al., 2010. skNAC, a Smyd1-interacting transcription factor, is involved in cardiac development and skeletal muscle growth and regeneration. Proc. Natl. Acad. Sci. U. S. A. 107, 20750–20755.
Peng, H., Hawrylycz, M., Roskams, J., Hill, S., Spruston, N., Meijering, E., et al., 2015. Big Neuron: large-scale 3D neuron reconstruction from optical microscopy Images. Neuron 87, 252–256. https://doi.org/10.1016/j.neuron.2015.06.036.
Pickrell, A.M., Huang, C.H., Kennedy, S.R., et al., 2015. Endogenous Parkin preserves dopaminergic substantia nigral neurons following mitochondrial DNA mutagenic stress. Neuron 87 (2), 371–381. https://doi.org/10.1016/j.neuron..06.034.
Rasmussen, T.L., Tucker, H.O., 2018. Loss of SMYD1 results in perinatal lethality via selective defects within myotonic muscle descendants. Diseases 7.
Rasmussen, T.L., et al., 2015. Smyd1 facilitates heart development by antagonizing oxidative and ER stress responses. PloS One 10, e0121765.
Raval, A., et al., 2012. Effect of nucleophosmin 1 haploinsufficiency on hematopoietic stem cells. Leukemia 26, 853–855.
Rhee, C., Lee, B.K., Beck, S., Anjum, A., Cook, K.R., Popowski, M., Kim, J., Tucker, H.O., 2014. Arid3a is essential to execution of the first cell fate decision via direct embryonic and extraembryonic transcriptional regulation. Genes Dev. 28 (20), 2219–2232. https://doi.org/10.1101/gad.247163.114, 15.
Riazi, Ali M., Lee, H., Hsu, C., Van Arsdell, G., 2005. CSX/Nkx 2.5 modulates differentiation of skeletal myoblasts and promotes differentiation into neuronal cells in vitro. J. Biol. Chem. 280, 10716–10720.
Sims 3rd, R.J., et al., 2002. m-Bop, a repressor protein essential for cardiogenesis, interacts with skNAC, a heart- and muscle-specific transcription factor. J. Biol. Chem. 277, 26524–26529.
EM Smyth, Grosser T, Wang M, Yu Y, FitzGerald GA. Prostanoids in health and disease. J. Lipid Res.. 50 Suppl. l:S423–S4282009.
Sprenkle, N.T., Sims, S.G., Sanchez, C.L., Meares, G.P., 2017. Endoplasmic reticulum stress and inflammation in the central nervous system. Mol. Neurodegener. 12 (1), 42–50.
Strang, K.H., Golde, T.E., Giasson, B.I., 2019. MAPT mutations, tauopathy, and mechanisms of neurodegeneration. Lab. Invest. 99, 912–928.
Talya, S., Neeraj, S., Lederkremer, G.Z., 2019. Protein misfolding and ER stress in Huntington's disease. Front. Mol. Biosci. 6, 1–20.
Tan, X., Rotllant, J., Li, H., De Deyne, P., Du, S.J., 2006. SmyD1, a histone methyltransferase, is required for myofibril organization and muscle contraction in zebrafish embryos. Proc. Natl. Acad. Sci. U. S. A. 103, 2713–2718.
Tracy, C., Warren, J.S., Szulik, M., Wang, L., Garcia, J., Makaju, A., Russell, K., Miller, M., Franklin, S., 2018. The Smyd family of methyltransferases: role in cardiac and skeletal muscle physiology and pathology. Current opinion in physiology 1, 140–152.
Uddin, M.S., Ghulam, A., 2018. Alzheimer's Disease-The Most Common Cause of Dementia. https://doi.org/10.5772/intechopen.82196.
Uemura, K., Hayashi, M., Itsubo, T., Oishi, A., Iwakawa, H., Komatsu, M., Uchiyama, S., Kato, H., 2017. Myostatin promotes tenogenic differentiation of C2C12 myoblast cells through Smad 3. FEBS Open Bio 7, 522–532.
Uylings, H.B.M., Van Pelt, J., Verwer, R.W.H., McConnell, P., 1989. Statistical analysis of neuronal populations. In: Capowski, J.J. (Ed.), Computer Techniques in Neuroanatomy. Springer, New York, NY, pp. 241–264.

Watanabe, Y., Kameoka, S., Gopalakrishnan, V., et al., 2004. Conversion of myoblasts to physiologically active neuronal phenotype. Genes Dev. 18 (8), 889–900.
Yahalom, V., Pillar, N., Zhao, Y., Modan, S., Fang, M., Yosephi, L., Asher, O., Shinar, E., Celniker, G., Resnik, W.H., Brantz, Y., Hauschner, H., Rosenberg, N., Cheng, L., Shomron, N., Pras, E., 2018. SMYD1 is the underlying gene for the AnWj-negative blood group phenotype. Eur. J. Haematol. 101 (4), 496–501.
Ye, X., Qian, Y., Wang, Q., et al., 2016. SMYD1, an SRF-interacting partner, Is involved in angiogenesis. PloS One 11 (1), e0146468.
Yotov, W.V., St-Arnaud, R., 1996. Differential splicing-in of a proline-rich exon converts alphaNAC into a muscle-specific transcription factor. Genes Dev. 10, 1763–1772.